Biomechan Model Mechanobiol (2007) 6:361–371
DOI 10.1007/s10237-006-0068-4

REVIEW

Cell traction force and measurement methods

James H-C. Wang · Jeen-Shang Lin

Received: 1 September 2006 / Accepted: 30 November 2006 / Published online: 3 January 2007

Abstract Cell traction forces (CTFs) are crucial to many biological processes such as inflammation, wound healing, angiogenesis, and metastasis. CTFs are generated by actomyosin interactions and actin polymerization and regulated by intracellular proteins such as alpha-smooth muscle actin (α-SMA) and soluble factors such as transforming growth factor-β (TGF-β). Once transmitted to the extracellular matrix (ECM) through stress fibers via focal adhesions, which are assemblies of ECM proteins, transmembrane receptors, and cytoplasmic structural and signaling proteins (e.g., integrins), CTFs direct many cellular functions, including cell migration, ECM organization, and mechanical signal generation. Various methods have been developed over the years to measure CTFs of both populations of cells and of single cells. At present, cell traction force microscopy (CTFM) is among the most efficient and reliable method for determining CTF field of an entire cell spreading on a two-dimensional (2D) substrate surface. There are currently three CTFM methods, each of which is unique in both how displacement field is extracted from images and how CTFs are subsequently estimated. A detailed review and comparison of these methods are presented. Future research should improve CTFM methods such that they can automatically track dynamic CTFs, thereby providing new insights into cell motility in response to altered biological conditions. In addition, research effort should be devoted to developing novel experimental and theoretical methods for determining CTFs in three-dimensional (3D) matrix, which better reflects physiological conditions than 2D substrate used in current CTFM methods.

Keywords Cell traction force microscopy · Optical flow · Correlation · Boussinesq solution · FEM

J. H-C. Wang (✉)
MechanoBiology Laboratory, Departments of Orthopaedic Surgery, Bioengineering and Mechanical Engineering,
E1640 Biomedical Science Tower,
210 Lothrop Street, Pittsburgh, PA 15213, USA
e-mail: wanghc@pitt.edu

J.-S. Lin
Department of Civil and Environmental Engineering
University of Pittsburgh, Pittsburgh, PA, USA

1 Introduction

In order to survive and grow, cells such as fibroblasts (Wang et al. 2001; Yang et al. 2006) and smooth muscle cells (Tolic-Norrelykke and Wang 2005; Wang et al. 2006) must attach to and spread on a substrate. Once attached, these cells generate internal tensile forces through actomyosin interactions and exert tractions on the underlying substrate or extracellular matrix (ECM). This cell traction force (CTF) is essential for cell migration, cell shape maintenance, mechanical signal generation, and other cellular functions. As such, CTF plays a key role in many biological processes, including inflammation, wound healing, embryogenesis, angiogenesis, and metastasis. Therefore, a complete knowledge of CTF regulation and the ability to measure CTFs are critical in understanding physiological and pathological events at both the tissue and organ levels. In this article, we will first provide a brief discussion of CTF in non-muscle cells, in terms of the role of different types of focal adhesions (FAs) and alpha-smooth muscle actin (α-SMA) in transmission and regulation of CTFs, respectively. Then we will describe existing methods for CTF measurement, with a detailed discussion of cell

traction force microscopy (CTFM). We conclude this review by suggesting future research directions for the improvement of CTFM technology and its potential biological applications.

2 Cell traction force

Non-muscle cells contain bundles of actin filaments, or "stress fibers," which form semi-sarcomere structures. Powered by ATP hydrolysis, the actomyosin cross-bridges inside these structures generate tension that contracts the cell body (Kolega et al. 1991; Sanger et al. 1983). This tension is then transmitted to the ECM, and the force exerted on the ECM is termed CTF (Fig. 1).

A second source for generating CTFs is actin polymerization that drives forward protrusion of the leading edge of a migrating cell (Bereiter-Hahn 2005; Elson et al. 1999). The traction forces are relayed to the ECM by FAs, which are located at both ends of the stress fiber and on the substrate or the ECM (Balaban et al. 2001) and hence physically connect the actin cytoskeleton to the ECM. The traction force at FA is in the range of tens of nano-Newtons (Burton et al. 1999; Lee et al. 1994; Tan et al. 2003).

FA is an assembly of ECM proteins, transmembrane receptors, and cytoplasmic structural and signaling proteins, including $\alpha v\beta 3$ and $\alpha 5\beta 1$ integrins, vinculin, paxillin, talin, zyxin, tensin, protein tyrosine kinases, and phosphatases (Geiger and Bershadsky 2001; Zamir and Geiger 2001). Among these FA proteins, integrins are primary mediators that provide a physical linkage between the actin cytoskeleton and ECM and thus play a pivotal role in cellular mechanotransduction (Ingber 2003; Wang et al. 1993).

Upon formation at the cell periphery, FAs are small, dot-like contacts also known as focal complexes (FCs),

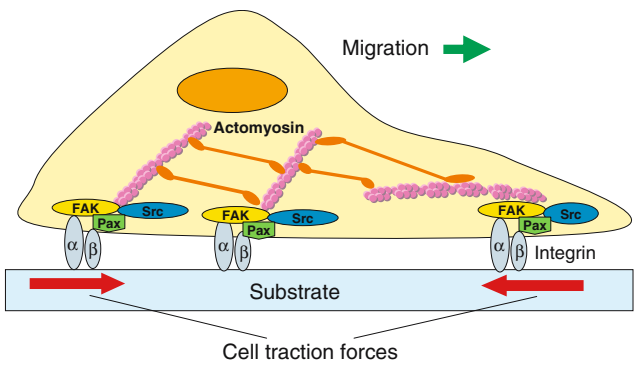

Fig. 1 An illustration of CTF in an adherent cell. CTFs are generated through the actomyosin interactions and act on the underlying substrate through focal adhesion proteins such as integrins

which are precursors of mature FAs (Beningo et al. 2001; Dugina et al. 2001; Riveline et al. 2001; Rottner et al. 1999). Large, mature FAs, also referred to as "classical" FAs (cFAs), are elongated, streak-like structures that link stress fibers at their ends (Goffin et al. 2006; Riveline et al. 2001). These FAs may develop into "supermature" FAs (suFAs), which are highly elongated cylindrical assemblies. "Supermature" FAs presumably result from the fusion of a few adjacent cFAs and are always associated with α-SMA-positive bundles of stress fibers (Dugina et al. 2001; Goffin et al. 2006), which form when cells are cultured on flat rigid substrates in vitro (Burridge and Chrzanowska-Wodnicka 1996) or when fibroblasts differentiate into myofibroblasts during wound healing (Tomasek et al. 2002).

Besides their differences in size, cFAs also differ from suFAs in molecular composition. cFAs consist of paxillin, vinculin, and phosphotyrosine (Zamir and Geiger 2001), whereas suFAs contain high levels of $\alpha 5\beta 1$ integrin, tensin, and other fibrillar adhesion proteins (Goffin et al. 2006). Additionally, the protein tyrosine phosphorylation level of paxillin and focal adhesion kinases (FAKs) in suFAs is significantly higher than that in cFAs, although total protein expression levels are similar in both (Goffin et al. 2006). Because of their differences in size and molecular composition, the three types of FAs (FCs, cFAs, and suFAs) behave distinctively in transmitting forces between a cell and an ECM substrate. It should be noted that substrate stiffness also affects formation of FAs, cytoskeletal structure (Yeung et al. 2005), and generation of CTFs (Kong et al. 2005; Lo et al. 2000).

As mentioned earlier, adherent cells generate contractile forces by actomyosin contractile machinery, and these forces are transmitted to the ECM through FAs. On the cFAs of relatively stationary cells, the magnitude of CTF linearly correlates with FA size (Balaban et al. 2001; Tan et al. 2003). On suFAs, however, CTF is markedly enhanced. In such cases, the average force per unit area of FA is about four times that observed in cFAs. This phenomenon is most likely attributed to the significantly higher level of protein tyrosine phosphorylation in suFAs (Goffin et al. 2006). Interestingly, however, cells also exert significantly larger forces on small FCs (less than 1 μm^2 in area); here the level of force no longer correlates with adhesion size (Tan et al. 2003). In particular, near the leading edge of a migrating fibroblast, small nascent FCs transmit strong propulsive traction forces, whereas large, mature FAs exert weak forces (Beningo et al. 2001); however, a differential finding is also reported (Galbraith et al. 2002). On the other hand, the FAs at the rear end only generate passive resistance during cell migration (Munevar et al.

2001b). Therefore, changes in the structure, molecular composition, and level of phosphorylation accompanied with the maturation of a FA result in a shift of its function from transmitting force for strong propulsion to maintaining spread cell morphology as a passive anchorage apparatus (Beningo et al. 2001).

Since CTF is generated through actomyosin interactions and actin polymerization forces, it is, therefore, regulated by two categories of molecules: those that regulate stress fiber/FA assembly such as Rho-kinase/ROCK (Watanabe et al. 1999) and those that regulate nonmuscle myosin II such as MLCK (Hartshorne et al. 1998). A detailed discussion of CTF-related regulation mechanisms can be found in an excellent recent review (Li et al. 2005). In recent years, however, α-SMA has emerged as a key molecule that upregulates CTF in myofibroblasts (Herman 1993; Serini and Gabbiani 1999). Unlike fibroblasts, myofibroblasts express α-SMA and incorporate it into stress fibers, and they also generate large traction forces (Grinnell 1994; Hinz et al. 2001). These large traction forces facilitate wound closure, ECM repair, and ECM remodeling; however, elevated traction forces from over-persistence of myofibroblasts can also lead to wound contracture, fibrosis, and other fibroproliferative disorders (Gabbiani 2003).

It has been demonstrated that α-SMA expression upregulates myofibroblast traction force in work using cell-populated collagen gel (CPCG) and thin silicone membrane (Hinz et al. 2001). Chen et al. (2006) have used CTFM to quantify traction forces generated by individual myofibroblasts and found that α-SMA protein expression is not necessary for generating CTF, but it does enhance CTF level in a nearly linear fashion.

Despite their importance, the mechanisms by which α-SMA protein expression enhance the generation of myofibroblast traction force are still not completely understood, although they likely relate to modification of stress fibers and FAs. For instance, α-SMA is enriched in stress fibers and at FA sites of myofibroblasts (Hinz et al. 2001) and allows the formation of suFAs to transmit large traction force (Goffin et al. 2006; Wang et al. 2006). In addition, the incorporation of α-SMA into actin filaments may enhance force transmission between cortical actin filaments and FAs (Dugina et al. 2001; Hinz et al. 2001, 2003). The specific N-terminal sequence of α-SMA, AcEEED, has been discovered to be crucial for incorporation of α-SMA into stress fibers and for force generation (Chaponnier et al. 1995; Clement et al. 2005). High levels of α-SMA expression not only enhance stress fiber formation, but may also increase CTF by Rho-dependent activation (Bogatkevich et al. 2003; Skalli et al. 1990). Moreover, α-SMA expression may mediate more efficient contraction by optimizing the spatial distribution of several subcellular forces (Hinz et al. 2001).

It is well known that TGF-β upregulates α-SMA expression and hence promotes myofibroblast differentiation of fibroblastic cells (Desmouliere et al. 1993; Evans et al. 2003; Kopp et al. 2005; Leask and Abraham 2004; Roy et al. 2001). TGF-β-induced α-SMA expression, however, also requires the induction of ED-A form of fibronectin (ED-A FN) and signaling molecules of the SMAD family (Kobayashi et al. 2006; Moustakas et al. 2001; Serini et al. 1998). Additionally, recent studies have found that TGF-β1 and TGF-β3, two isoforms of TGF-β, induce differential α-SMA expression and myofibroblast traction force. For instance, TGF-β1 induces higher α-SMA expression and traction force than TGF-β3 in human patellar tendon fibroblasts (Campbell et al. 2004). On the other hand, soluble factors such as bFGF, PGE_2, and γ-interferon inhibit TGF-β1-upregulated α-SMA expression and thus likely cause the downregulation of CTF (Burgess et al. 2005; Hjelmeland et al. 2004; Kawai-Kowase et al. 2004; Kolodsick et al. 2003).

3 Methods for cell traction force measurement

3.1 Cell-populated collagen gel (CPCG)

In this method, cells are mixed with collagen gel, typically bovine collagen type I. Once polymerized, a gel disk is obtained. Due to CTFs generated by embedded cells, the gel contracts and the diameter of the disk decreases (Bell et al. 1979; Ehrlich 1988; Moon and Tranquillo 1993). CTFs can then be estimated by measuring change in diameter of the gel disk. A subsequent development introduces cell force monitor, in which a free-floating CPCG is held in place and CTFs are quantified using strain gauges (Campbell et al. 2003; Delvoye et al. 1991). Despite its elegance, this approach does not measure traction forces of individual cells (Ferrenq et al. 1997); instead, it measures gel contraction caused by the traction forces from a population of embedded cells. It is known that CTF generation depends on substrate rigidity (Lo et al. 2000), which changes as the CPCG shrinks. Other parameters, such as composition and number of cells in the gel, also undergo continuous change as the embedded cells actively remodel the collagen gel, thus introducing further variables. All these factors cause complications in measuring CTFs by CPCG method.

3.2 Thin silicone membrane

The use of thin silicone membrane introduces another method to measure CTFs. Applying this technique,

Harris et al. (1981) demonstrated that individual fibroblasts generate traction forces, as evidenced by the fact that cells create wrinkles on thin silicone membrane. Later, this approach was used to determine traction forces generated during cytokinesis of individual cells using a calibration technique (Burton and Taylor 1997). Force applied to the thin silicone membrane by an adherent cell is estimated by applying a flexible microneedle to reverse the wrinkles. The needle stiffness is measured by hanging weights fabricated with small glass beads. However, as wrinkling presents an inherently non-linear problem, there is currently no suitable computational method to accurately predict the wrinkles caused by a complex, non-isotropic traction force field generated by a single cell.

3.3 Force sensor array

This method uses a micro-machined device consisting of an array of cantilever beams that is fabricated using lithography (Galbraith and Sheetz 1997). When a CTF is applied, it bends a cantilever beam. From the extent of bending recorded, the traction force is determined based on the beam deflection-force relationship obtained through calibration. This method can quantify CTF in one direction, but it is limited in that it cannot determine the traction forces in all directions within the entire cell spreading area.

An improved method, termed micropost force sensor array (MFSA), has been recently developed for measuring CTFs (du Roure et al. 2005; Tan et al. 2003). Each micropost in the MFSA works as an individual force-sensing unit and independently measures local CTFs applied by the cell. One advantage of the MFSA over micro-cantilevers (Galbraith and Sheetz 1997) is that it can detect traction forces of individual cells or a cell monolayer in all directions.

The use of micropatterned elastomer by Balaban et al. (2001) represents an important innovation. The surface topology of an elastometer is modulated with micro-dots of 0.3 μm in height that serve as markers for determination of substrate deformation from analysis of phase contrast images. The traction force at each focal adhesion is obtained by solving an inverse problem using elasticity theory. The use of the micropatterned elastomers simplifies the determination of the cell traction induced displacement field. However, the stiffness of silicone membrane cannot be adjusted low enough to sense small deformations. With a variation of the ratio of the silicone elastomer to curing agent from 50:1 to 10:1, Young's modulus of the elastometer varies between 12 and 1,000 kPa (Schwarz et al. 2002). In contrast, polyacrylamide gel (PG) can be made more compliant. By changing the proportion of acrylamide and bis-monomers, Young's modulus of PG may vary from 1.2 to 100 kPa (Butler et al. 2002; Wang and Pelham 1998). The PG gel also has the advantages of being highly elastic, transparent, mechanically stable, and easy to prepare. These desirable properties make it an excellent substrate material for CTFM. Both micropatterned elastomers and PG substrates are modeled as flat elastic substrates in CTF analysis. As such, procedures used in recovering CTFs from substrate deformation, as described below, apply to both cases.

4 Cell traction force microscopy (CTFM)

The current CTFM methods, which use elastic PG substrate in measuring CTFs, follow a decoupled approach and involve three major steps. The first step is to fabricate elastic PG substrate with a flat surface. The next step is to obtain a pair of "null force" and "force loaded" microscopy images, from which the displacement field is determined based on the movement of markers on the surface of the PG substrate. In the final step, the substrate deformation is used to compute CTFs. The current approaches can be represented by three different methods that were developed by Dembo and Wang (DW) (1999), Butler et al. (2002), and Yang et al. (2006), respectively. Current CTFM methods that use flat PG substrates have a common first step but differ in the second and the third steps.

4.1 Fabricating PG substrate and imaging cells

A PG substrate is a gel disk that is prepared in a circular dish by mixing fluorescent microbeads with acrylamide/bis-acrylamide that has a pre-determined bis-acrylamide to acrylamide ratio. The gel disk is further coated with collagen type I before cells are plated on it. Several separate cells in each dish are chosen for imaging at different time intervals on an inverted microscope. This yields "force loaded" images. The cells in the dish are detached afterwards by trypsinization, and an image of the same location is taken. This is denoted as the "null force" image.

4.2 Determining substrate displacement field

The fluorescent microbeads serve as markers for tracking the movement of the substrate under CTFs. By locating the microbeads in the images taken before and after straining PG substrate, microbead movements are determined. In contrast to micropatterned elastomers, the unstructured microbeads in PG require matching

(Fig. 2). The image change due to microbead movement is referred to as *optical flow* (Sonka et al. 1993). To match pixels between these two images are equivalent to finding a proper mapping function for the optical flow at each pixel of the "null force" image. Each pixel on an image has a gray value characterized often by an 8-bit integer, and the brighter the pixel, the higher its gray value. The fluorescent microbeads may be identified, at least in theory, because they are brighter than background, but it is a challenging task in practice. One complicating factor is that there are simply too many microbeads, on the order of a few thousand, within each image. Thus, instead of dealing with microbeads directly, Dembo and Wang (1999) and Butler et al. (2002) rely on the similarity in area contrast between a pair of images to identify substrate deformation.

In the Butler et al. method, optical flow is constructed not on a pixel basis, but rather in an average sense of a small window. For instance, on a $1,024 \times 1,280$ pixel image, the typical window size used is 64×64 pixels. Butler et al. divided each image into overlapped windows with a constant distance, such as 16 pixels, between successive windows. One window in the "null-force" image is matched to that in the "force-loaded" image provided these two windows give the highest cross correlation. A displacement is defined as the distance between the centers of these two windows. The correlation computation is carried out using Fourier transform. The main steps of the procedure include:

1. Image correction: Compute cross correlation between the whole null-force image, I_0, and the force-loaded image, I_1, and translate one image against the other so that the pixels with maximum correlation are matched.
2. A fixed size window, typically of 64×64 pixels, moves over each image such that successive windows are overlapped by a fixed distance such as 16 pixels.
3. For each window in image I_0, a cross correlation is computed against a window occupying the same coordinates in image I_1.
4. The coordinates of the peak cross-correlation function is assigned to the center of the window in I_0 as its displacement vector.
5. Repetitive application of the process gives the displacement field.
6. For window pairs that give small cross-correlation, displacement values are discarded. Instead, a third order polynomial fitting of their neighborhoods are employed to generate displacements as replacement.

The DW method uses a correlation-based "optical flow" algorithm (Marganski et al. 2003). This method, like the Butler et al. method, also starts by setting a grid on the "null force" image with the objective only to estimate the movement of these grid points. But the DW approach is more flexible, as the displacement is not restricted to be between two fixed windows. The procedure is detailed below:

1. Set up the parameters: (a) lattice size, (b) window half-size, C, (c) search distance, S, and (d) a maximum level of strain norm, $\varepsilon_{\max}$.
2. Cover the null-force image, I_0, with a lattice, and determine the locations of the lattice nodes. For each lattice node, n, select an initial guess of the matching point, m, in the force-loaded image, I_1. The set of all pixels that lie within a distance S from m, $\{m\}$, contains the candidates for matching.
3. Correlation windows of fixed size of $2C \times 2C$, with n and each pixel in $\{m\}$ as the respective centers, are employed to obtain contrast correlations. The pixel

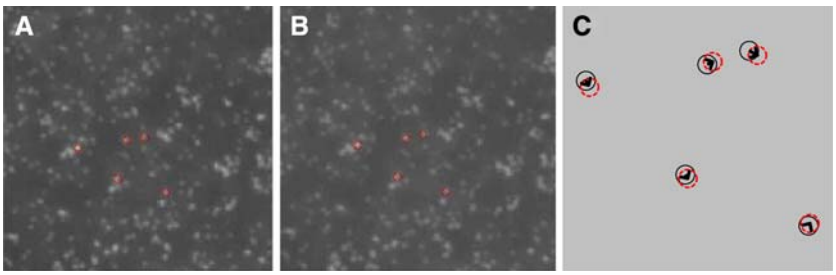

Fig. 2 **a** A partial fluorescent bead image (150×150 pixels) after cell detachment. This image is denoted "null force" image, with several microbeads marked. **b** The same fluorescent bead image before cell detachment. This image is denoted "force loaded" image. A matching algorithm is needed to match a pair of microbeads between the "force loaded" image and the "null force" image. This matching is used to compute the substrate displacement field from which CTFs are subsequently determined. **c** The displacements of the selected microbeads. They are determined as the distances between the centers of the matched microbeads

in $\{m\}$ that gives the highest correlation with n is considered a near optimal matching point.
4. A quadratic interpolation around this near optimal is further carried out to obtain the best matching point, m, in I_1 for n in I_0.
5. Compute the in-plane strain norm and if that exceeds the strain norm $\varepsilon_{\max}$, correlation window size is doubled and the matching is repeated.
6. After removing rigid body mode, the distance between n and m gives the displacement of n.
7. A repetitive application of the procedure gives the displacement field.

The use of a rectangular window, however, prohibits both the DW and Butler et al. approaches from taking into account any local rotation mode of displacement.

Yang et al. (2006) present a different approach by attempting to identify the optical flow of microbeads. This procedure, through the adoption of a local threshold, first distinguishes a microbead from its background. A summary of the procedure is given here:

1. Pre-select the parameters: maximum levels of displacements, $d_{\max}$, normal strains $\varepsilon_{\max}$, and shear strains, $\gamma_{\max}$.
2. The first step is to identify discernable beads by requiring a potential bead to be a cluster that is greater than 4 but less than 8 pixels:
   (a) Each image is divided into small windows of 16×16 pixels so that average contrast in each window is obtained.
   (b) The image is turned into binary so that each pixel brighter than the local average becomes 1, and 0 otherwise.
   (c) The one-clusters that have sizes larger than 4 and less than 8 pixels are identified as beads.
3. Matching beads from null-force image, I_0, and the force-loaded image, I_1:
   (a) Start with an arbitrary bead, u_0, in I_0, and find its closest neighboring bead, u_1. Connect the two beads with a line segment, l_0.
   (b) At the corresponding locations in image I_1, one circle each is drawn with u_0 and u_1 as the center, respectively, with a radius of $d_{\max}$. Connect each bead in the first circle with one bead in the second circle. Each line segment so formed, l_{i}, is compared with l_0 for the magnitudes of elongation and rotation. The l_i that best satisfies both the elongation and rotation criteria is considered a match.
   (c) If no match is found, another u_1 point is selected until a match is found or no match can be found. If a match is found, the bead pair is recorded and the displacement computed.
   (d) The computation continues, using u_1 as the new u_0 point, until all beads in I_0 have been used.

The displacement field is then corrected to eliminate the rigid body mode. This is done by fitting the far field displacement data. Mismatch of microbeads may be reduced by requiring the bead movement to be locally smooth.

One common problem to all three of these methods is that the quality of the displacement field deteriorates as the microbeads become more sparsely distributed. Moreover, the error of the estimated displacement field is difficult to quantify. In Yang et al.'s approach, however, it is possible to conduct a spot check in which one can manually calculate displacements of selected microbeads, as Fig. 2 illustrates.

4.3 Determining cell traction forces

In the determination of CTFs from the estimated displacement field, one needs to make a decision on the proper formulation to adopt and the extent of the displacement field to incorporate. Choosing a proper formulation is crucial because the recovery of traction force represents an inverse problem. It has been stated that such an inverse problem is ill-posed and requires regularization (Schwarz et al. 2002). According to Hadamard (1923), a problem which fails to meet any of the following three conditions is ill-posed: (1) a solution always exists, (2) the solution is unique, and (3) the solution to the problem depends continuously on the data of the problem. This last condition basically requires a system to be stable and that a small perturbation in the displacement measurements should not induce a large variation in the resulting forces. However, Butler et al. (2002) and Yang et al. (2006) have been able to tackle the problem successfully without explicit regularization. Their approaches dictate that both the forces and displacements be set on grids or meshes, which can be viewed as an implicit form of regularization in that high frequency components has been truncated and thus limits the level of perturbation in traction forces due to noises. This is further explained in the discussion that follows. Explicit regularization comes with a higher computational cost, but one gains more control with the ability to impose effects of noises, or tune the characteristics of resulting forces.

A forward model is also needed in formulating an inverse problem. All the forward models utilize the fact

that PG gel substrates behave as linear elastic media (Pelham and Wang 1997) and employ elasticity theory. Most researchers have been using the simple yet elegant Boussinesq analytical solution (Landau and Lifshitz 1986) as the forward model. The Boussinesq solution gives the surface displacement of an infinite half-space due to a point surface load. Since the substrate is of finite thickness, such an application of the Boussinesq solution is bound to introduce errors. Yang et al. (2006) evaluated such error by 3D FEM analysis of a PG gel substrate plate subjected to a point load. The substrate plate has a surface area of 1,000 μm × 1,000 μm and a thickness that varies from 1,000, 200, to 70 μm, respectively. Their results show that under a given load, substrate thickness significantly affects the induced displacements both in how fast they decay and also in their magnitudes. For the thick 1,000 μm substrate, excluding the singularity at the loading point, FEM and Boussinesq solutions are close as expected. However, as the substrate becomes thinner, the displacement decays faster than $1/r$, and its magnitude also gets smaller (Yang et al. 2006). That is to say that for a thin substrate, the Boussinesq solution gives displacement larger than its FEM counter part that considers actual substrate thickness. Conversely, the Boussinesq solution would project a smaller force given a displacement when far field data are used. The error of using Boussinesq solution in the far field on a thin substrate is substantial. This casts uncertainty in the inclusion of far field data for the estimation of CTFs.

In applying the Boussinesq solution, the expected displacement at any point, $\mathbf{x}_i$, of an elastic substrate due to n CTFs can be expressed in a general discrete convolution form. The displacement vector $\mathbf{d}_i$ at a point $\mathbf{x}_i$ due to various force vectors $\mathbf{F}_j$ at all $\mathbf{x}_j$ can be expressed as follows:

$$\mathbf{d}_i = \sum_{j=1}^{m} \mathbf{G}(\mathbf{r}_{ij})\mathbf{F}_j \tag{1}$$

where both $\mathbf{d}_i$ and $\mathbf{F}_j$ are vectors containing x and y components, and $\mathbf{r}_{ij} = \mathbf{x}_i - \mathbf{x}_j$ is a distance vector. In a general form, the Boussinesq solution for the displacement at r away from a force can be written as

$$\mathbf{G}(\mathbf{r}) = \frac{1+\nu}{\pi E r^3}\begin{bmatrix} (1-\nu)r^2 + \nu\, r_x^2 & \nu\, r_x r_y \\ \nu\, r_x r_y & (1-\nu)r^2 + \nu\, r_y^2 \end{bmatrix} \tag{2}$$

where $r = \sqrt{\mathbf{r}\cdot\mathbf{r}}$, $\mathbf{r} = (r_x, r_y)$, E is Young's modulus, and ν the Poisson's ratio of the elastic substrate.

Collecting all the convolution equations from each of the n displacement points gives a simultaneous equation between the m force vectors and the n displacement vectors. The recovery of the traction force field is to obtain these m force vectors given the n displacement vectors. In the following, three approaches are discussed. They are developed by Butler et al., Dembo and Wang, and Yang et al., respectively.

4.4 Butler et al.'s approach

Butler et al. (2002) make use of the property that through a Fourier transform (FT), a convolution equation becomes a simple multiplication. That is, the displacement convolution equation, Eq. (1), after FT becomes a simple multiplication as follows:

$$\bar{\mathbf{d}}(\mathbf{k}) = \bar{\mathbf{G}}(\mathbf{k}) \cdot \bar{\mathbf{F}}(\mathbf{k}) \tag{3}$$

where the upper bar denotes a FT quantity and k denotes a radial wave vector. Butler et al. have derived elegantly the FT of the Boussinesq equation in an analytical form as

$$\bar{\mathbf{G}}(\mathbf{k}) = \frac{2(1+\nu)}{Ek^3}\begin{bmatrix} (1-\nu)k^2 + \nu k_y^2 & \nu k_x k_y \\ \nu k_x k_y & (1-\nu)k^2 + \nu k_x^2 \end{bmatrix} \tag{4}$$

where $\mathbf{k} = (k_x, k_y)$ and $k = \sqrt{k_x^2 + k_y^2}$.

Posing this way, the FT of a traction force can be found by a simple inversion

$$\bar{\mathbf{F}}(\mathbf{k}) = \bar{\mathbf{G}}(\mathbf{k})^{-1} \cdot \bar{\mathbf{d}}(\mathbf{k}) \tag{5}$$

It can be readily seen that as $\mathbf{k}$ increases, each term in $\bar{\mathbf{G}}(\mathbf{k})$ decays with 1/k, whereas its inverse, $\bar{\mathbf{G}}(\mathbf{k})^{-1}$, reverses the trend, and its value increases with k. Should $\mathbf{k}$ become very large, the noises in the displacement could be substantially amplified by $\bar{\mathbf{G}}(\mathbf{k})^{-1}$ into the resulting force and the problem becomes ill-posed. By using a regular grid, Butler et al. limit the highest value of $\mathbf{k}$ and thus avoid potential problems of ill-conditioning. This is what we referred to as an implicit regularization in the preceding discussion.

A traction force is obtained in three steps. First, FT is carried out on the displacement field. Second, the FT of the traction force at each wave number is obtained using the preceding equation. Third, an inverse FT operation, or IFT, on the whole field then gives the traction forces.

As their displacements are estimated over a grid, the periodicity requirement of FT is satisfied. However, FT of the Boussinesq has a singularity at $\mathbf{k} = 0$. A simple way to overcome this singularity is to truncate its value at $\mathbf{k} = 0$ and thus remove the singularity.

Two force recovery approaches were proposed. The *unconstrained method* does not confine the locations of traction forces. It considers all the displacement data and allows the traction forces to locate anywhere on the grid irrespective of the location of a cell. Basically, it utilizes all displacement data in FT, and after inversion obtains

the FT of the forces. The force field is obtained with a subsequent application of IFT. On the other hand, the *constrained method* does restrict the traction forces to be located only within the cell boundary. This requires iteration. In each iteration, a traction force field is first obtained using the unconstrained method. The forces located outside the boundary of the cell are set to zero, and the displacements from the modified forces computed. The approach then replaces the computed displacement field under the cell with the measured values. That is equivalent to discarding the measured displacement data outside the cell. In the next iteration, the unconstrained method is again applied on this modified displacement field. Iteration continues until the traction forces within the cell converge.

The unconstrained method has the benefit of not having to know the boundary of a cell, but it is difficult to justify its use, as one cannot justify the underlying reasoning that a traction force can locate anywhere even very far from the cell. In Butler et al's approach, the recovered traction forces are most likely complex numbers. This requires the imaginary part to be neglected, which may result in additional errors.

4.5 Dembo and Wang's approach

Dembo and Wang (1999) pose the traction force recovery problem as a regularized parameter estimation problem. They first discretize the interior of a cell with a mesh, and consider traction forces to apply on the mesh nodes. As the number of measured displacements, m, is much larger than the number of traction forces, n, one cannot simply obtain traction forces through inversion. A parameter estimation scheme is needed to estimate the traction forces. As governing equation may be ill-conditioned, a Tikhonov regularization is introduced, and their estimate is formulated as a minimization of the following term

$$\chi^2 + \lambda I^2 \tag{6}$$

where χ^2 is the chi-square statistic, which is a square error measure defined as follows:

$$\chi^2 = \sum_{i=1}^{n} \frac{\left(\mathbf{d}_i - \sum_{j=1}^{m} \mathbf{G}(\mathbf{r}_{ij})\mathbf{F}_j\right)^2}{\sigma_i^2} \tag{7}$$

and σ_i represents the estimated error in measurement of the ith displacement; λ is the Tikhonov regularization parameter, and I^2 is a constraint. DW adopted a constraint which dictates that the traction field be smooth. To solve the problem, they started with $\lambda = 0$ and progressively increased it until the results gave an unacceptable χ^2. This approach is flexible, and different constraints of I^2 can be employed or added. In their application, they used all available displacement data.

Schwarz et al. (2002), while using micropatterned elastomers, also applied regularization in estimating CTFs but have formulated the forces as unknowns at discrete adhesion points which were identified as the centers of GFP-vinculin clusters from fluorescence images.

4.6 Yang et al.'s approach

Yang et al. (2006), instead of adopting Boussinesq solution, used 3D FEM so that the effects of finite substrate thickness are incorporated. A forward FEM formulation adopts an adequate interpolation function and, with a subsequent application of Galerkin method (Zienkiewicz et al. 2005), poses a problem such that forces are known and displacements are to be found.

In case the displacements are known, such as in the present application, forces can be directly computed without inversion. Yang et al. (2006) built a 3D FEM model of a finite thickness substrate using a regular lattice, upon which the fixed boundary condition is imposed on all the nodes at the base of the substrate. The rest of the nodes are either traction free or are prescribed with known displacements. They introduced prescribed displacements only to the nodes on the substrate surface in contact with the cell. In this way, a solution is further simplified through static condensation. A static condensation expresses the displacements at the traction-free nodes as a function of those at the prescribed displacement nodes. This dependency leads to a reduced degree of freedom, and CTFs can be obtained through multiplication.

The procedure of the FEM approach is equivalent to Butler et al.'s constrained method, but with two significant advantages: there is no need for iteration and the finite thickness of the substrate is considered. The 3D FEM computation is very efficient. Because of the use of a regular lattice, not much overhead is introduced for the meshing task. A typical force computation including meshing using five layers of elements along the depth with a mesh size of 4 μm × 4 μm on each layer surface, or an equivalent of about 9,000 nodes, takes less than 1 min with a 1.2 GHz Pentium PC using a commercial software ANSYS (Fig. 3).

In the process of estimating CTFs, DW utilized both near field and far field displacement data, while Butler et al.'s constrained method and Yang et al. employed only the near field data. The argument for DW approach is that discarding far-field data is equivalent to discarding valuable information. On the other hand, the use of the static condensation advocates that

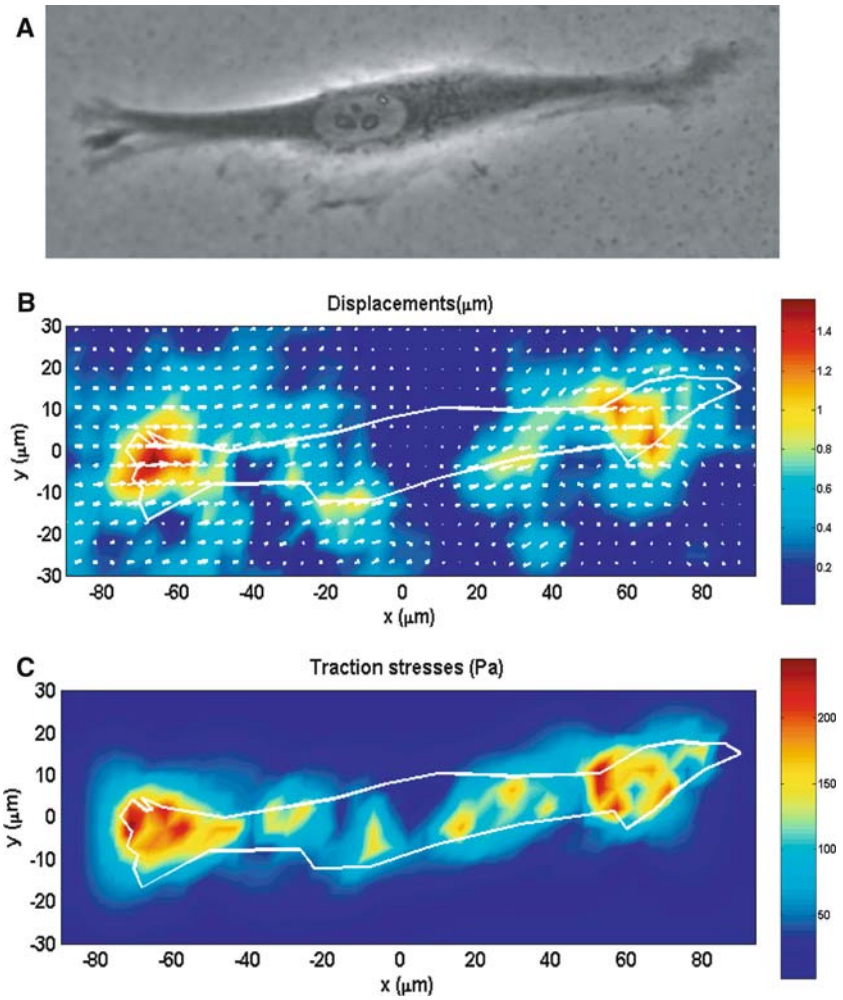

Fig. 3 A typical example of applying a matching algorithm to determine the substrate displacement field and a 3D FEM analysis to determine CTFs. **a** Human patellar tendon fibroblast on a polyacrylamide gel with embedded fluorescent beads (not shown). **b** Substrate displacement field. **c** Recovered CTF field (adopted from Fig. 6 in Yang et al. 2006, J Theor Biol 242:607–616)

the displacements decay from a cell at a fast rate of $1/r$, as such the noise may render the far-field data not essential.

5 Concluding remarks

CTF is necessary for an adherent cell to migrate, maintain its shape, organize ECM, probe physical environments, and generate mechanical signals. It is well recognized that a detailed knowledge of CTF is crucial in understanding many fundamental biological processes, including embryogenesis, angiogenesis, and metastasis. For example, in tumorigenesis and metastasis, elevated traction force is found in activated fibroblasts (Kalluri and Zeisberg 2006), and transformed cells have lesser traction forces than their non-transformed counterparts (Harris et al. 1981; Munevar et al. 2001a). The role of traction force in cancers, however, is not well understood and remains to be explored by CTF measurement methods.

Currently, among many measurement methods, CTFM provides the most reliable, comprehensive information on CTFs underlying an entire cell. Significant advances in CTF measurement methods have been made in the last decade, though these methods still have much room for improvement in terms of reducing errors in estimating CTFs and improving computational efficiency. A comparative study of various methods using the same data set may be one way to quantify the differences in the resulting CTFs. Moreover, because the current procedures treat estimation of displacement and cell traction fields as separate decoupled processes, a possible improvement would be to combine the two as a single process. Further, current CTFM methods must also be improved to achieve automation and real-time tracking of CTFs, which will provide new information on dynamic cell behavior under various biological conditions. Additionally, CTFM methods will have much broader application if they are extended to more physiologically-representative 3D matrices, rather than being limited to 2D substrate surfaces as they currently are. One potential application of CTFM methods is to quantify CTF and use it as a "biophysical marker" to characterize phenotypic changes in individual cells under altered biological conditions.

Acknowledgment We thank Mr. Michael Lin for his assistance in preparing this review. We also gratefully acknowledge the funding support of NIH grant AR049921 and the Arthritis Investigator Award (JHW).

References

Balaban NQ, Schwarz US, Riveline D, Goichberg P, Tzur G, Sabanay I, Mahalu D, Safran S, Bershadsky A, Addadi L, Geiger B (2001) Force and focal adhesion assembly: a close relationship studied using elastic micropatterned substrates. Nat Cell Biol 3(5):466–472

Bell E, Ivarsson B, Merrill C (1979) Production of a tissue-like structure by contraction of collagen lattices by human fibroblasts of different proliferative potential in vitro. Proc Natl Acad Sci USA 76(3):1274–1278

Beningo KA, Dembo M, Kaverina I, Small JV, Wang YL (2001) Nascent focal adhesions are responsible for the generation of strong propulsive forces in migrating fibroblasts. J Cell Biol 153(4):881–888

Bereiter-Hahn J (2005) Mechanics of crawling cells. Med Eng Phys 27(9):743–753

Bogatkevich GS, Tourkina E, Abrams CS, Harley RA, Silver RM, Ludwicka-Bradley A (2003) Contractile activity and smooth muscle alpha-actin organization in thrombin-induced human lung myofibroblasts. Am J Physiol Lung Cell Mol Physiol 285(2):L334–L343

Burgess HA, Daugherty LE, Thatcher TH, Lakatos HF, Ray DM, Redonnet M, Phipps RP, Sime PJ (2005) PPARgamma agonists inhibit TGF-beta induced pulmonary myofibroblast differentiation and collagen production: implications for therapy of lung fibrosis. Am J Physiol Lung Cell Mol Physiol 288(6):L1146–L1153

Burridge K, Chrzanowska-Wodnicka M (1996) Focal adhesions, contractility, and signaling. Annu Rev Cell Dev Biol 12:463–518

Burton K, Taylor DL (1997) Traction forces of cytokinesis measured with optically modified elastic substrata. Nature 385(6615):450–454

Burton K, Park JH, Taylor DL (1999) Keratocytes generate traction forces in two phases. Mol Biol Cell 10(11):3745–3769

Butler JP, Tolic-Norrelykke IM, Fabry B, Fredberg JJ (2002) Traction fields, moments, and strain energy that cells exert on their surroundings. Am J Physiol Cell Physiol 282(3):C595–C605

Campbell BH, Clark WW, Wang JH (2003) A multi-station culture force monitor system to study cellular contractility. J Biomech 36(1):137–140

Campbell BH, Agarwal C, Wang JH (2004) TGF-beta1, TGF-beta3, and PGE(2) regulate contraction of human patellar tendon fibroblasts. Biomech Model Mechanobiol 2(4): 239–245

Chaponnier C, Goethals M, Janmey PA, Gabbiani F, Gabbiani G, Vandekerckhove J (1995) The specific NH2-terminal sequence Ac-EEED of alpha-smooth muscle actin plays a role in polymerization in vitro and in vivo. J Cell Biol 130(4):887–895

Chen J, Li H, SundarRaj N, Wang JH (2006) Alpha-smooth muscle actin expression enhances cell traction force. Cell Motil Cytoskeleton (in press)

Clement S, Hinz B, Dugina V, Gabbiani G, Chaponnier C (2005) The N-terminal Ac-EEED sequence plays a role in alpha-smooth-muscle actin incorporation into stress fibers. J Cell Sci 118(Pt 7):1395–1404

Delvoye P, Wiliquet P, Leveque JL, Nusgens BV, Lapiere CM (1991) Measurement of mechanical forces generated by skin fibroblasts embedded in a three-dimensional collagen gel. J Invest Dermatol 97(5):898–902

Desmouliere A, Geinoz A, Gabbiani F, Gabbiani G (1993) Transforming growth factor-beta 1 induces alpha-smooth muscle actin expression in granulation tissue myofibroblasts and in quiescent and growing cultured fibroblasts. J Cell Biol 122(1):103–111

Dugina V, Fontao L, Chaponnier C, Vasiliev J, Gabbiani G (2001) Focal adhesion features during myofibroblastic differentiation are controlled by intracellular and extracellular factors. J Cell Sci 114(Pt 18):3285–3296

Ehrlich HP (1988) The role of connective tissue matrix in wound healing. Prog Clin Biol Res 266:243–258

Elson EL, Felder SF, Jay PY, Kolodney MS, Pasternak C (1999) Forces in cell locomotion. Biochem Soc Symp 65: 299–314

Evans RA, Tian YC, Steadman R, Phillips AO (2003) TGF-beta1-mediated fibroblast-myofibroblast terminal differentiation-the role of Smad proteins. Exp Cell Res 282(2):90–100

Ferrenq I, Tranqui L, Vailhe B, Gumery PY, Tracqui P (1997) Modelling biological gel contraction by cells: mechanocellular formulation and cell traction force quantification. Acta Biotheor 45(3–4):267–293

Gabbiani G (2003) The myofibroblast in wound healing and fibrocontractive diseases. J Pathol 200(4):500–503

Galbraith CG, Sheetz MP (1997) A micromachined device provides a new bend on fibroblast traction forces. Proc Natl Acad Sci USA 94(17):9114–9118

Galbraith CG, Yamada KM, Sheetz MP (2002) The relationship between force and focal complex development. J Cell Biol 159(4):695–705

Geiger B, Bershadsky A (2001) Assembly and mechanosensory function of focal contacts. Curr Opin Cell Biol 13(5):584–592

Goffin JM, Pittet P, Csucs G, Lussi JW, Meister JJ, Hinz B (2006) Focal adhesion size controls tension-dependent recruitment of alpha-smooth muscle actin to stress fibers. J Cell Biol 172(2):259–268

Grinnell F (1994) Fibroblasts, myofibroblasts, and wound contraction. J Cell Biol 124(4):401–404

Hadamard J (1923) Lectures on the cauchy problem in linear partial differential equations. Yale University Press

Harris AK, Stopak D, Wild P (1981) Fibroblast traction as a mechanism for collagen morphogenesis. Nature 290(5803):249–251

Hartshorne DJ, Ito M, Erdodi F (1998) Myosin light chain phosphatase: subunit composition, interactions and regulation. J Muscle Res Cell Motil 19(4):325–341

Herman IM (1993) Actin isoforms. Curr Opin Cell Biol 5(1):48–55

Hinz B, Celetta G, Tomasek JJ, Gabbiani G, Chaponnier C (2001) Alpha-smooth muscle actin expression upregulates fibroblast contractile activity. Mol Biol Cell 12(9):2730–2741

Hinz B, Dugina V, Ballestrem C, Wehrle-Haller B, Chaponnier C (2003) Alpha-smooth muscle actin is crucial for focal adhesion maturation in myofibroblasts. Mol Biol Cell 14(6):2508–2519

Hjelmeland MD, Hjelmeland AB, Sathornsumetee S, Reese ED, Herbstreith MH, Laping NJ, Friedman HS, Bigner DD, Wang XF, Rich JN (2004) SB-431542, a small molecule transforming growth factor-beta-receptor antagonist, inhibits human glioma cell line proliferation and motility. Mol Cancer Ther 3(6):737–745

Ingber DE (2003) Mechanosensation through integrins: cells act locally but think globally. Proc Natl Acad Sci USA 100(4):1472–1474

Kalluri R, Zeisberg M (2006) Fibroblasts in cancer. Nat Rev Cancer 6(5):392–401

Kawai-Kowase K, Sato H, Oyama Y, Kanai H, Sato M, Doi H, Kurabayashi M (2004) Basic fibroblast growth factor antagonizes transforming growth factor-beta1-induced smooth muscle gene expression through extracellular signal-regulated kinase 1/2 signaling pathway activation. Arterioscler Thromb Vasc Biol 24(8):1384–1390

Kobayashi T, Liu X, Wen FQ, Kohyama T, Shen L, Wang XQ, Hashimoto M, Mao L, Togo S, Kawasaki S, Sugiura H, Kamio K, Rennard SI (2006) Smad3 mediates TGF-beta1-induced collagen gel contraction by human lung fibroblasts. Biochem Biophys Res Commun 339(1):290–295

Kolega J, Janson LW, Taylor DL (1991) The role of solation-contraction coupling in regulating stress fiber dynamics in nonmuscle cells. J Cell Biol 114(5):993–1003

Kolodsick JE, Peters-Golden M, Larios J, Toews GB, Thannickal VJ, Moore BB (2003) Prostaglandin E2 inhibits fibroblast to myofibroblast transition via E. prostanoid receptor 2 signaling and cyclic adenosine monophosphate elevation. Am J Respir Cell Mol Biol 29(5):537–544

Kong HJ, Polte TR, Alsberg E, Mooney DJ (2005) FRET measurements of cell-traction forces and nano-scale clustering of adhesion ligands varied by substrate stiffness. Proc Natl Acad Sci USA 102(12):4300–4305

Kopp J, Preis E, Said H, Hafemann B, Wickert L, Gressner AM, Pallua N, Dooley S (2005) Abrogation of transforming growth factor-beta signaling by SMAD7 inhibits collagen gel contraction of human dermal fibroblasts. J Biol Chem 280(22):21570–21576

Landau LD, Lifshitz EM (1986) Theory of elasticity. Pergamon, Oxford

Leask A, Abraham DJ (2004) TGF-beta signaling and the fibrotic response. Faseb J 18(7):816–827

Lee J, Leonard M, Oliver T, Ishihara A, Jacobson K (1994) Traction forces generated by locomoting keratocytes. J Cell Biol 127(6 Pt 2):1957–1964

Li S, Guan JL, Chien S (2005) Biochemistry and biomechanics of cell motility. Annu Rev Biomed Eng 7:105–150

Lo CM, Wang HB, Dembo M, Wang YL (2000) Cell movement is guided by the rigidity of the substrate. Biophys J 79(1):144–152

Marganski WA, Dembo M, Wang YL (2003) Measurements of cell-generated deformations on flexible substrata using correlation-based optical flow. Meth Enzymol 361:197–211

Moon AG, Tranquillo RT (1993) Fibroblast–populated collagen microsphere assay of cell traction force .1. Continuum model. Aiche J 39(1):163–177

Moustakas A, Souchelnytskyi S, Heldin CH (2001) Smad regulation in TGF-beta signal transduction. J Cell Sci 114(Pt 24):4359–4369

Munevar S, Wang Y, Dembo M (2001a) Traction force microscopy of migrating normal and H-ras transformed 3T3 fibroblasts. Biophys J 80(4):1744–1757

Munevar S, Wang YL, Dembo M (2001b) Distinct roles of frontal and rear cell-substrate adhesions in fibroblast migration. Mol Biol Cell 12(12):3947–3954

Pelham RJ Jr, Wang Y (1997) Cell locomotion and focal adhesions are regulated by substrate flexibility. Proc Natl Acad Sci USA 94(25):13661–13665

Riveline D, Zamir E, Balaban NQ, Schwarz US, Ishizaki T, Narumiya S, Kam Z, Geiger B, Bershadsky AD (2001) Focal contacts as mechanosensors: externally applied local mechanical force induces growth of focal contacts by an mDia1-dependent and ROCK-independent mechanism. J Cell Biol 153(6):1175–1186

Rottner K, Hall A, Small JV (1999) Interplay between Rac and Rho in the control of substrate contact dynamics. Curr Biol 9(12):640–648

du Roure O, Saez A, Buguin A, Austin RH, Chavrier P, Silberzan P, Ladoux B (2005) Force mapping in epithelial cell migration. Proc Natl Acad Sci USA 102(7):2390–2395

Roy SG, Nozaki Y, Phan SH (2001) Regulation of alpha-smooth muscle actin gene expression in myofibroblast differentiation from rat lung fibroblasts. Int J Biochem Cell Biol 33(7):723–734

Sanger JW, Sanger JM, Jockusch BM (1983) Differences in the stress fibers between fibroblasts and epithelial cells. J Cell Biol 96(4):961–969

Schwarz US, Balaban NQ, Riveline D, Bershadsky A, Geiger B, Safran SA (2002) Calculation of forces at focal adhesions from elastic substrate data: the effect of localized force and the need for regularization. Biophys J 83(3):1380–1394

Serini G, Gabbiani G (1999) Mechanisms of myofibroblast activity and phenotypic modulation. Exp Cell Res 250(2):273–283

Serini G, Bochaton-Piallat ML, Ropraz P, Geinoz A, Borsi L, Zardi L, Gabbiani G (1998) The fibronectin domain ED-A is crucial for myofibroblastic phenotype induction by transforming growth factor-beta1. J Cell Biol 142(3):873–881

Skalli O, Gabbiani F, Gabbiani G (1990) Action of general and alpha-smooth muscle-specific actin antibody microinjection on stress fibers of cultured smooth muscle cells. Exp Cell Res 187(1):119–125

Sonka M, Hlavac V, Boyle R (1993) Image processing, analysis and machine vision, vol xix Chapman & Hall, London, p 555

Tan JL, Tien J, Pirone DM, Gray DS, Bhadriraju K, Chen CS (2003) Cells lying on a bed of microneedles: an approach to isolate mechanical force. Proc Natl Acad Sci USA 100(4):1484–1489

Tolic-Norrelykke IM, Wang N (2005) Traction in smooth muscle cells varies with cell spreading. J Biomech 38(7):1405–1412

Tomasek JJ, Gabbiani G, Hinz B, Chaponnier C, Brown RA (2002) Myofibroblasts and mechano-regulation of connective tissue remodelling. Nat Rev Mol Cell Biol 3(5):349–363

Wang N, Butler JP, Ingber DE (1993) Mechanotransduction across the cell surface and through the cytoskeleton. Science 260(5111):1124–1127

Wang YL, Pelham RJ Jr (1998) Preparation of a flexible, porous polyacrylamide substrate for mechanical studies of cultured cells. Methods Enzymol 298:489–496

Wang HB, Dembo M, Hanks SK, Wang Y (2001) Focal adhesion kinase is involved in mechanosensing during fibroblast migration. Proc Natl Acad Sci USA 98(20):11295–11300

Wang J, Zohar R, McCulloch CA (2006) Multiple roles of alpha-smooth muscle actin in mechanotransduction. Exp Cell Res 312(3):205–214

Watanabe N, Kato T, Fujita A, Ishizaki T, Narumiya S (1999) Cooperation between mDia1 and ROCK in Rho-induced actin reorganization. Nat Cell Biol 1(3):136–143

Yang Z, Lin JS, Chen J, Wang JH (2006) Determining substrate displacement and cell traction fields-a new approach. J Theor Biol 242:607–616

Yeung T, Georges PC, Flanagan LA, Marg B, Ortiz M, Funaki M, Zahir N, Ming W, Weaver V, Janmey PA (2005) Effects of substrate stiffness on cell morphology, cytoskeletal structure, and adhesion. Cell Motil Cytoskeleton 60(1):24–34

Zamir E, Geiger B (2001) Molecular complexity and dynamics of cell-matrix adhesions. J Cell Sci 114(Pt 20):3583–3590

Zienkiewicz OC, Taylor RL, Nithiarasu P, Zhu JZ (2005) The finite element method: its basis and fundamentals. Butterworth-Heinemann